Atmos. Chem. Phys. Discuss., https://doi.org/10.5194/acp-2018-322
Manuscript under review for journal Atmos. Chem. Phys.
Discussion started: 2 May 2018

Atmospheric Chemistry and Physics Discussions

Long-term trends of global marine primary and secondary aerosol production during the recent global warming hiatus (2000-2015)

Sang-Keun Song[a], Zang-Ho Shon[b,*], Yu-Na Choi[a], Young-Baek Son[c], Minsung Kang[b], Seung-Beom Han[a], Min-Suk Bae[d]

[a] *Department of Earth and Marine Sciences, Jeju National University, Jeju 63243, Republic of Korea*

[b] *Department of Environmental Engineering, Dong-Eui University, Busan 47340, Republic of Korea*

[c] *Jeju International Marine Science Center for Research & Education, Korea Institute of Ocean Science & Technology (KIOST), Jeju 63349, Republic of Korea*

[d] *Department of Environmental Engineering, Mokpo National University, Muan 58554, Republic of Korea*

Abstract

Long-term trends in global sea spray aerosol (SSA) emissions and dimethyl sulfide (DMS) fluxes from sea to air during the recent global warming hiatus (2000–2015) were analyzed using satellite observations and modelling data. The SSA emissions were estimated using a widely used whitecap method with sea surface temperature (SST) dependence. In addition, sea-to-air DMS fluxes were also used to quantify the secondary contributions of DMS through its sequential oxidation and gas-to-particle conversion. Aerosol optical depth (AOD) was estimated by an aerosol optical model using the number concentration of SSA and non-sea-salt sulfate from DMS. The estimated AOD, which was derived from the SSA and DMS emitted from the sea surface, was compared with satellite-derived AOD to quantify its (primary and secondary) contribution to atmospheric aerosol loading (i.e., observed AOD). Yearly global mean anomalies in DMS fluxes and AOD derived from SSA showed statistically significant downward trends during the recent global warming hiatus, whereas SSA emissions and AOD derived

*Corresponding author: Dept. of Environment Engineering, Dong-Eui University, 995 Eom Gwang No, Busan Jin Gu, Busan 47340, Republic of Korea; E-mail: zangho@deu.ac.kr; Tel: +82-51-890-2078; Fax: +82-51-890-2076

Atmos. Chem. Phys. Discuss., https://doi.org/10.5194/acp-2018-322
Manuscript under review for journal Atmos. Chem. Phys.
Discussion started: 2 May 2018

Atmospheric Chemistry and Physics Discussions

from DMS oxidation did not. In terms of regional trends, the decreases in SSA emissions during 2000–2015 occurred over the central Pacific Ocean, the Indian Ocean, and the Caribbean Sea, whereas upward trends in SSA emissions occurred over the tropical southeastern Pacific Ocean, the Southern Ocean, and the North Atlantic Ocean. DMS fluxes during the study period showed a clear downward trend over most regions of the global ocean. The estimates of the contributions of SSA (primary) and DMS (secondary) to atmospheric aerosol loading were 23–62% and 26–38%, respectively, with the largest primary contribution (~90%) over the Southern Ocean.

Keywords: Sea spray aerosol, DMS, Trend, MODIS AOD, OPAC

Atmos. Chem. Phys. Discuss., https://doi.org/10.5194/acp-2018-322
Manuscript under review for journal Atmos. Chem. Phys.
Discussion started: 2 May 2018

Atmospheric Chemistry and Physics Discussions

1. Introduction

Over the past few decades, the Earth's climate system has undergone substantial changes due to increases in atmospheric concentrations of greenhouse gases (GHGs) and aerosols from anthropogenic sources (IPCC, 2013). It is certain that the increase in GHG concentrations has, since the late 19th century, caused the global mean surface air temperature (SAT) to rise, with a warming of 0.85°C from 1880 to 2012 (IPCC, 2013). However, the rate of warming (0.05°C per decade) over the last 15 years (1998–2012) was smaller than that (0.12°C per decade) calculated for 1951–2012 (IPCC, 2013). According to a recent study (England et al., 2014), the global mean SAT has remained flat since around 2001, reflecting a hiatus in global warming, possibly due to increased subsurface ocean heat uptake, the cool sea surface temperature (SST) in the eastern Pacific, and changes in atmospheric water vapor and aerosols.

Excluding black carbon, atmospheric aerosols act to counter the global warming effects of GHGs and play an important role in the Earth's climate system due to their direct and indirect effects on the Earth's radiative balance (IPCC, 2013). Marine aerosols, one of the most important natural aerosol systems, includes sea spray aerosol (SSA) that is formed at the sea surface primarily through the breaking of waves via bubble bursting (Blanchard, 1963) and, at elevated wind speeds, the direct tearing of wave crests (Monahan et al., 1986). In addition, the non-sea-salt (NSS) sulfate (SO_4^{2-}) fraction of marine aerosol is produced by the gas-to-particle conversion of dimethyl sulfide (DMS), emitted from the sea surface in the marine boundary layer (Saltzman et al., 1986). Global emissions of natural SSA (2,200 to 118,000 Tg yr^{-1}) are significantly larger than those of anthropogenic aerosols (111 Tg yr^{-1} in 2010, Klimont et al., 2017), despite their large uncertainty, which is due to the difficulty of parameterizing SSA emissions (de Leeuw et al., 2011 and references therein).

Interestingly, the variations in SSA emissions over the tropical Pacific Ocean were affected by changing sea surface wind (SSW) and SST associated with the El Niño-Southern Oscillation (ENSO) variability and were highly correlated with changes in aerosol optical depth (AOD) (Yang et al., 2016). A significant influence of oceanic DMS emissions on cloud condensation nuclei (CCN) concentrations was reported from November–April, whereas a strong influence of SSA emissions on CCN was reported

during austral winter over the remote Southern Ocean (Korhonen et al., 2008). Strong coupling between annual cycles of methanesulfonic acid, which is produced by the oxidation of DMS, CCN, and satellite-derived AOD, was also observed at Gape Grim (40°41′S, 144°41′E) (Gabric et al., 2002).

The atmospheric aerosol mass loading from natural and anthropogenic sources can be represented by the AOD, which is the degree to which aerosols prevent the transmission of light by absorption or scattering of radiation (i.e., the integrated extinction coefficient over the atmospheric column). Thus, concentrations/emissions (or production) of aerosols of marine origin (e.g., SSA and NSS-SO_4^{2-}), and anthropogenic aerosols, may be related closely to AOD observations. A number of studies on aerosols related to climate change have focused on issues related to radiative forcing by changes in anthropogenic aerosol emissions (e.g., nitrate, sulfate, mineral, dust, organic carbon, and black carbon) (IPCC, 2013). Global anthropogenic emissions of particulate matter (PM_{10}) increased from 56974 Gg yr^{-1} in 2000 to 60651 Gg yr^{-1} in 2010 (6.5% increase) (Klimont et al., 2017). However, an understanding of the long-term variation in the production of natural marine aerosols, as well as their primary and secondary contributions to atmospheric aerosol loadings (e.g., AOD) in the marine atmosphere, is limited. Thus, the aim of this study was to analyze the long-term trends in global SSA emissions and DMS fluxes during the recent global warming hiatus period (2000–2015). In addition, we evaluated the long-term variations of separate aerosol loadings derived from primary (SSA) and secondary (DMS oxidation) marine aerosols. Finally, we estimated their contributions to satellite-observed AOD.

2. Materials and methods

2.1 Estimation of SSA emissions

To examine the long-term trend in global marine aerosol fluxes and its contribution to atmospheric aerosol loading, including indirect contributions, it was necessary to estimate SSA emissions and sea-to-air DMS fluxes over the global ocean. The emission strength of SSA has been parameterized from semi-empirical combinations of whitecap factorization and concentration measurements (Monahan et al., 1986; Smith and Harrison, 1998; Gong, 2003; Clarke et al., 2006). In the literature, SSA source functions of Monahan et al. (1986) and Gong (2003) have been widely used in the estimation of global SSA emissions. Other parameters, including SST, wave height, and salinity, have been known to affect

Atmos. Chem. Phys. Discuss., https://doi.org/10.5194/acp-2018-322
Manuscript under review for journal Atmos. Chem. Phys.
Discussion started: 2 May 2018

Atmospheric Chemistry and Physics Discussions

SSA emission processes such as initial air entrainment, buoyancy of air bubbles, and bubble size spectra, which are partially responsible for the discrepancies between different studies (Mårtensson et al., 2003; Ovadnevaite et al., 2014; Salter et al., 2014; Grythe et al., 2014; de Leeuw et al., 2011; Jaeglé et al., 2011).

In this work, size-dependent SSA emissions were estimated using the parameterization of Gong (2003), with the third-order SST dependence from Jaeglé et al. (2011):

$$\frac{dF}{dr_{80}} = A_{SST}\,1.373 U_{10}^{3.41} r_{80}^{-B} (1 + 0.057 r_{80}^{3.45}) \times 10^{C}$$

$$A_{SST} = 0.3 + 0.1T - 0.0076T^2 + 0.00021T^3$$

$$B = 4.7(1 + \Theta r_{80})^{-0.017 r_{80}^{-1.44}}$$

$$C = 1.607 \exp\left(-\left[\frac{0.433 - \log r_{80}}{0.433}\right]^2\right)$$

where dF/dr_{80} ($m^{-2}\,s^{-1}$) is the SSA number flux, r_{80} (μm) is the aerosol radius at 80% relative humidity, which is taken as a typical value in the marine boundary layer, U_{10} ($m\,s^{-1}$) is the wind speed at 10 m, and Θ (30) is an adjustable shape parameter that controls the submicron size distribution. Monthly U_{10} datasets at 25-km spatial resolution were obtained from the Quick Scatterometer (QuikSCAT) satellite for 2000–2007, and the Advanced Scatterometer (ASCAT) for 2008–2015, due to sensor failure or malfunction of the QuikSCAT. Monthly SST (T) datasets at 9-km spatial resolution were obtained from the NOAA Advanced Very High Resolution Radiometer (AVHRR) satellite for 2000–2002 and Aqua Moderate Resolution Imaging Spectroradiometer (MODIS) for 2003–2015, due to the unavailability of MODIS data for the first 3 years.

2.2 Estimation of DMS fluxes

Sea-to-air fluxes of DMS can be computed as the product of surface seawater DMS concentrations and the gas transfer velocity at the air–sea interface (Gabric et al., 2004; Archer et al., 2010). The basic equation used to estimate the DMS flux (F_{DMS}: μmol $m^{-2}\,day^{-1}$) is expressed as

$$F_{DMS} = k_w[DMS]_{aq}$$

Atmos. Chem. Phys. Discuss., https://doi.org/10.5194/acp-2018-322
Manuscript under review for journal Atmos. Chem. Phys.
Discussion started: 2 May 2018

Atmospheric Chemistry and Physics Discussions

where k_w is the sea-to-air transfer velocity (m s^{-1}) and $[DMS]_{aq}$ represents surface DMS concentrations (nM) in the seawater. In this study, monthly mean DMS fluxes over the global ocean during 2000–2015 were estimated using satellite-based data (e.g., chlorophyll a (Chl-a), SSW, and SST) and model-predicted mixed layer depths (MLDs). The $[DMS]_{aq}$ in the global ocean was estimated using an empirical algorithm constructed with Chl-a concentrations (mg m^{-3}) and MLDs (m) using the following equations (Kettle et al., 1999; Simó and Dachs, 2002; Cropp et al., 2004; Gabric et al., 2004):

$$[DMS]_{aq} = -\mathrm{Ln}(MLD) + 5.7 \qquad \text{Chl-a/MLD} < 0.02$$

$$[DMS]_{aq} = 55.8(\text{Chl-a/MLD}) + 0.6 \qquad \text{Chl-a/MLD} \geq 0.02$$

where the monthly Chl-a concentration was obtained from the Sea-Viewing Wide Field-of-View Sensor (SeaWiFS) for 2000–2002 and Aqua MODIS data for 2003–2015, at 9-km spatial resolution. In addition, the monthly MLD (1/6° resolution) in the global ocean was derived separately from several model-predicted datasets due to limited satellite data availability: Simple Ocean Data Assimilation (SODA) for 2000–2004, the Fleet Numerical Meteorology and Oceanography Center (FNMOC) for July 2005 to December 2008, and HYbrid Coordinate Ocean Model (HYCOM) data for 2009–2015.

In general, the gas transfer velocity from sea to air (k_w) is parameterized with wind speed (SSW) and molecular diffusivity (Schmidt number). Two types of parameterizations, Liss and Merlivat (1986) and Wanninkhof (1992), are used commonly in the literature. The former parameterizes the transfer velocity for three regimes of wind speed separately with a first-order equation (Liss and Merlivat, 1986), while the latter uses a second-order equation (Wanninkhof, 1992). In this study, the Liss and Merlivat (1986) approach was used to calculate DMS fluxes during the study period. We used the dependence of the Schmidt number (for DMS flux) on SST by Saltzman et al. (1993). Descriptions of the SST and SSW data are discussed in section 2.1. To match the resolution (25 km) of the SSW data, the Chl-a and SST data (9-km resolution) and the MLD data (1/6° resolution) were converted into 25-km resolution data using MATLAB and Fortran. Detailed information on the calculation of transfer velocities and the associated DMS fluxes has been described in previous studies (Liss and Merlivat, 1986; Wanninkhof, 1992; Cropp et al., 2004; Gabric et al., 2004; Kettle and Merchant, 2005).

2.3 Estimation of the contributions of marine aerosols to atmospheric aerosol loading

Atmos. Chem. Phys. Discuss., https://doi.org/10.5194/acp-2018-322
Manuscript under review for journal Atmos. Chem. Phys.
Discussion started: 2 May 2018

Atmospheric Chemistry and Physics Discussions

144 The contributions of primary SSAs, emitted from the sea surface, and secondary NSS-SO_4^{2-}
145 aerosols, produced by DMS oxidation, to atmospheric aerosol loadings over the marine atmosphere were
146 estimated using the calculation of the AOD derived from both aerosol types. AOD (or AOD_{SSA}) derived
147 from SSA emission was calculated using the aerosol size distribution over the ocean described by Lewis
148 and Schwartz (2004), which was parameterized with U_{10}:

149 $$\frac{dN}{d\log r_{80}} = 0.07U_{10}^{2}\exp\left(-\frac{1}{2}\left[\frac{\ln r_{80}-\ln r_i}{\ln \sigma_i}\right]^2\right)$$

150 where $dN/dlog\ r_{80}$ (cm^{-3}) is the size distribution at a relative humidity of 80%, r_i is the count median
151 particle radius (0.21 μm), σ_i is a geometric standard deviation (2.03), and r_{80} is in the range 0.07–20 μm.
152 The count median radius and geometric standard derivation were calculated by fitting the size
153 distribution of SSA emission derived from the Gong (2003) parameterization. The Optical Properties of
154 Aerosols and Clouds (OPAC) model was used to calculate the AOD. Detailed information on the OPAC
155 is given by Hess et al. (1998). In brief, the OPAC model provides the microphysical and optical
156 properties of aerosols and clouds in the solar and terrestrial spectral range (e.g., 61 wavelengths of 0.25–
157 40 μm for aerosols and water clouds). The optical properties of aerosol particles and cloud droplets were
158 modeled using Mie theory, assuming spherical particles (Quenzel and Müller, 1978).

159 AOD (or AOD_{DMS}) derived from the secondary marine aerosol (e.g., NSS-SO_4^{2-}) was estimated
160 using the default condition for the clean maritime aerosol type (water-soluble part originating from gas-
161 to-particle conversion) in the OPAC model of Hess et al. (1998), with consideration of a weighting
162 factor based on the global distribution of DMS fluxes. For example, the default total number
163 concentration was assigned to the global mean DMS flux. For this simulation, a lognormal size
164 distribution was assumed, with a count median radius of 0.0212 μm, a geometric standard deviation of
165 2.24, and total number concentrations of 1500 cm^{-3} (for the water-soluble part of the clean maritime
166 aerosol type). An observation or the SO_4^{2-} number concentration in the accumulation mode over the
167 Arabian Sea indicated that it reached a maximum value of 1800 cm^{-3} (Verma et al., 2012). Given that
168 our total number concentration is in the range of previously observed values, the value assigned is
169 reasonable for the estimation of AOD_{DMS}. Finally, the AOD_{SSA} and AOD_{DMS} simulated by the OPAC

model were compared with MODIS satellite-based observations of AOD, to quantify the primary and secondary contributions, respectively.

3. Results and Discussion

3.1 Long-term trends and distributions of global SSA emissions and DMS fluxes

Figures 1 and 2 show the geographical distribution of the long-term annual trends and anomalies in the annual means for SSA emissions, DMS fluxes, SSW, and SST over the global ocean from January 2000 to December 2015. There was no statistically significant global annual trend in SSA emissions for 2000–2015 (Fig. 2). However, the long-term trends in SSA emissions did exhibit regional differences during the study period. An upward trend in SSA emissions occurred over the tropical southeastern Pacific Ocean (especially at 5°N–23°S and 70°W–110°W), the northeastern Pacific (15°N–30°N, 120°W–140°W), the Southern Ocean (40°S–60°S), and the North Atlantic Ocean (45°N–60°N, 0°–60°W). The maximum and mean slopes in the tropical southeastern Pacific Ocean were +0.03 and +0.01 g m^{-2} yr^{-1}, respectively. A downward trend in SSA emissions occurred over the tropical Pacific Ocean, the Indian Ocean, and the Caribbean Sea, with mean slopes of −0.012, −0.013, and −0.0099 g m^{-2} yr^{-1}, respectively. In contrast to SSA emissions, there was a statistically significant downward trend (−10.2 μg m^{-2} yr^{-1}, R^2 = 0.68) in global DMS fluxes during the study period (Fig. 2). In addition, DMS fluxes for 2000–2015 exhibited a clear downward trend over most oceans, except for the slight upward trend over the tropical South Pacific Ocean.

In general, the geographical distributions of the long-term trends in SSA emissions and DMS fluxes were similar to that of SSW, but are somewhat different from those of SST, Chl-a, and DMS concentrations, due to their strong dependences on wind speed (i.e., $U_{10}^{3.41}$ for SSA emissions and U_{10} for DMS fluxes). Thus, the long-term SST trend did not significantly affect SSA emissions and DMS fluxes. The global average SST has remained mostly steady since 2001, with little regional variation, despite ongoing increases in atmospheric GHGs (IPCC, 2013). Two of the most recent extended hiatus periods (1940–1975 and 2001–present) correspond closely to the negative phase of the Interdecadal Pacific Oscillation (IPO), which manifests as a low-frequency El Niño pattern of climate variability with

a cool tropical Pacific (Folland, et al., 2002; England et al., 2014). England et al. (2014) suggested that a key component of the most recent global warming hiatus was the cool eastern Pacific SST, due to the strengthening of Pacific trade winds over the past two decades, which causes an increase in equatorial upwelling, a decrease in SST, and a substantial slowdown in surface warming through increased subsurface ocean heat uptake.

The downward trend in SSA emissions (with a mean of −12 mg m^{-2} yr^{-1}) over the tropical Pacific Ocean (10°N–5°S and 180°W–120°W) was related strongly to the downward trend in SSW (−0.057 m s^{-1}), whereas the downward trend in DMS fluxes (−7.16 μmol m^{-2} yr^{-1}) over this region was not significant due to the combination of its weak SSW dependence (gas transfer velocity) and the compensating effect of increasing seawater DMS concentrations (+0.021 nM). The downward trend in DMS fluxes over this region was caused mainly by the downward trend in SSW (e.g., k_w). Yang et al. (2016) found that variations in sea salt emissions over the tropical Pacific Ocean were affected by changing wind speeds associated with ENSO variability. A recent satellite chlorophyll record indicated that trends in ocean chlorophyll (e.g., DMS) from September 1997 to December 2012 were upward (0.54–0.72% yr^{-1}) in this region (Hammond et al., 2017).

The long-term annual trends (or slopes) in SSA emissions and DMS fluxes were examined using the non-parametric statistical method of Mann–Kendall (hereinafter MK), through which monotonic trends (either increases or decreases) were evaluated along with Sen's non-parametric method for estimating the slope of a linear trend (Table 1 and Supplementary Table 1, respectively) (Simmonds, et al., 2004; Carslaw, 2005; Anttila and Tuoviene, 2010). In general, the statistically significant long-term trends in SSA emissions for the latitude bands (10° interval between 0° and 60°) over the global ocean for 2000–2015 were dependent on their geographic locations (Table 1). Clear upward and downward trends in annual SSA emissions were calculated in the Northern Hemisphere (NH). In the NH, an upward trend in SSA emissions (+0.074 mg m^{-2} yr^{-1} or 2.2% yr^{-1}) was calculated for the high latitudes (50°N–60°N), whereas downward trends (−0.070 to −0.23 mg m^{-2} yr^{-1} or −0.6 to −1.7% yr^{-1}) were calculated for latitudes below 40°N. In the Southern Hemisphere (SH), an upward trend (+0.15 mg m^{-2} yr^{-1} or 1.6% yr^{-1}) was calculated for the latitude band 50°S–60°S only. In addition, the yearly downward trends of

Atmos. Chem. Phys. Discuss., https://doi.org/10.5194/acp-2018-322
Manuscript under review for journal Atmos. Chem. Phys.
Discussion started: 2 May 2018

Atmospheric Chemistry and Physics Discussions

DMS fluxes at most latitudes in the NH and SH ranged from −4.7 to −13.1 (or −0.49 to −3.2% yr^{-1}) and −5.8 to −18.6 μmol m^{-2} yr^{-1} (or −1.1 to −4.2% yr^{-1}), respectively (Supplementary Table 1).

Long-term trends in SSA emissions for each latitude band in both the NH and the SH differed by season (Table 1). In the NH, most downward trends in SSA emissions (−3.48 to −24.3 μg m^{-2} yr^{-1} or −1.06 to −3.57% yr^{-1}) occurred at latitudes below 40°N during summer (JJA) and fall (SON), whereas clear upward trends were calculated in the latitude bands of 20°N–30°N during winter (DJF) (+0.27 mg m^{-2} yr^{-1} or 3.5% yr^{-1}) and 50°N–60°N during the spring (MAM) (+0.064 mg m^{-2} yr^{-1} or 5.5% yr^{-1}) and DJF (+0.47 mg m^{-2} yr^{-1}or 17.4% yr^{-1}). In the SH, however, the areas with statistically significant trends in SSA emissions were restricted to the specific latitude band for each season. Upward trends were predicted in the latitude bands of 10°S–20°S (+0.32 mg m^{-2} yr^{-1} or 1.1% yr^{-1}) during JJA and 50°S–60°S (+0.32 mg m^{-2} yr^{-1} or 4.9% yr^{-1}) during SON, whereas downward trends were predicted in the latitude bands of 0°S–20°S (−0.08 to 0.18 mg m^{-2} yr^{-1} or −0.6 to −0.8% yr^{-1}) during MAM, 30°S–40°S (−0.11 mg m^{-2} yr^{-1} or −2.2% yr^{-1}) during JJA, and 0°S–10°S during DJF (−0.09 mg m^{-2} yr^{-1} or −0.7% yr^{-1}).

In contrast to the varying SSA emission trends among latitudinal bands, DMS fluxes exhibited a downward trend globally (Supplementary Table 1, Choi, et al., 2017). A detailed discussion of the DMS flux trends is given by Choi et al. (2017). In the NH, the downward trends (−3.65 to −23.4 μmol m^{-2} yr^{-1} or −0.4 to −8.4% yr^{-1}) were predicted for latitudes below 50°N, regardless of season (except for DJF (−2.92 μmol m^{-2} yr^{-1} or −0.4% yr^{-1}) at 50°N–60°N). In the SH, the downward trend (−9.86 μmol m^{-2} yr^{-1} or −1.3% yr^{-1}) in the tropics was predicted during SON only. The relative decreases during DJF (−2.73 to −8.4% yr^{-1}) were significantly faster than those during other seasons (−0.51 to −2.0% yr^{-1}) due to large reductions in DMS concentrations (0.60 to 69% yr^{-1}).

Zone-averaged distributions of SSA emissions, DMS fluxes, SSW, and SST were calculated for 2000–2015 (Supplementary Fig. 1). In the NH, annual SSA emissions were highest over the latitude band 10°N–20°N (25 mg m^{-2} yr^{-1}) because this region had a high wind speed (5.9 m s^{-1}) and the second highest SST (27.0°C). For DMS fluxes, annual patterns in both the NH and the SH were generally higher at low latitudes than at mid-latitudes (except for 40°S–60°S), due primarily to the high SSW (≥6.0 m

s^{-1}) and, in part, the high SST (≥26°C). Our global mean DMS fluxes ranged from 12.1 Tg yr^{-1} (2000) to 10.7 Tg yr^{-1} (2015), which are similar to those derived from DMS measurements during 1972–1998 (15.0 Tg yr^{-1}, Kettle and Andreae, 2000) and during 1972–2009 (17.6 Tg yr^{-1}, Lana et al., 2011). The distribution of monthly mean wind speeds over the sea surface for 2015 was dominated by the range 4–8 m s^{-1}, accounting for 50% of the entire wind speed range. The most frequent oceanic wind speed range was 5–7 m s^{-1} (U_{10}, 3 h, 1° × 1°) with a long-tailed distribution towards higher wind speeds (Grythe et al., 2014). SSA emissions (9.6–25 mg m^{-2} yr^{-1}) at low latitudes (0°N–30°N) were significantly higher than those (1.8–3.2 mg m^{-2} yr^{-1}) at mid-latitudes (40°N–60°N) due to high wind speeds and high SST. On average, wind speeds (4.6–5.9 m s^{-1}) at low latitudes were a factor of 1.6 higher than those (3.0–3.6 m s^{-1}) at mid-latitudes, while surface temperatures (24.5°C–27.7°C) at low latitudes were a factor of 2.0 higher than those (8.1°C–19.9°C) at mid-latitudes.

In both the NH and the SH, there were no significant differences in seasonal SSA emissions for the mid latitudes (30°–60°) during 2000–2015 (data not shown). However, there were large differences in seasonal SSA emissions at low latitudes (30°N–30°S). For instance, winter SSA emissions (32 and 31 mg m^{-2} yr^{-1} for the NH and SH, respectively) were highest in the 10°–20° latitude band of both hemispheres due to the high winter wind speeds in this region, whereas the lowest SSA emissions for the NH were predicted at 50°N–60°N during JJA (0.7 mg m^{-2} yr^{-1}), and at 30°S–40°S (2.1 mg m^{-2} yr^{-1}) during SON. There was no significant difference in annual mean SSA emissions between the NH (9.9 mg m^{-2} yr^{-1}) and the SH (11.6 mg m^{-2} yr^{-1}). Monthly variations in SSA emissions in the NH exhibited two distinct peaks, in June and January or December at 0°–20°N, whereas there was a peak in July at 0°–20°S (data not shown).

3.2. Long-term trends and the distribution of AOD_{SSA} and AOD_{DMS}

AODs over the ocean are affected by direct SSA emissions and the chemical transformation of DMS emitted from the sea surface, the long-range transport of aerosols from continental regions, anthropogenic aerosols derived from ships, and dry and wet deposition. Figure 3 shows the long-term trends in AODs (τ_{550}) derived from SSA emissions (AOD_{SSA}) and DMS fluxes (AOD_{DMS}) during 2000–

2015. In general, the trends in AOD_{SSA} and SSA emissions were similar. Interestingly, the intensity of annual trends in AOD_{SSA} over the ocean was significantly different from that of SSA emissions, with a decreasing AOD trend. AOD is a function of the aerosol number concentrations, size distribution, and chemical composition and is less affected by the mass concentration of aerosols. The aerosol mass concentration is governed entirely by coarse particles (>1 μm), whereas the aerosol number concentration is dominated by fine particles (<1 μm). Thus, the trends of AOD_{SSA} were weak compared with those of SSA emissions (mass-based). Unlike the trend in SSA emissions, a statistically significant strong upward trend in AOD_{SSA} (+0.011 or 33.6% yr^{-1}) was predicted over the Sea of Okhotsk. In contrast to AOD_{SSA}, the AOD_{DMS} slopes were higher due to increases in DMS concentrations in seawater, especially in the tropics (+0.0009 or 1.48% yr^{-1}). Upward trends extended into the tropical Atlantic and Indian Oceans, similar to the distribution of DMS concentrations in seawater (Fig. 1).

In addition, a sensitivity study was conducted to explore the effects of wind speed (U_{10}) and/or an adjustment factor (Θ) on SSA emission and AOD_{SSA}. The sensitivity study revealed that a ±25% change in U_{10} gave a +114/−63% change in annual SSA emission rates and a +20/−16% change in AOD_{SSA}. The effects of changing the adjustment factor on the SSA emission rates and AOD were negligible (0.7% change in SSA emission after decreasing Θ from 30 to 8). Changing the default aerosol number concentration (1500 cm^{-3}) by 50% resulted in a 30% change in AOD_{DMS}. Finally, a 50% change in DMS flux resulted in a 30% change in AOD_{DMS}.

To compare the trends in natural marine AOD and total AOD (anthropogenic and natural), we analyzed the AOD (τ_{550}) trends derived from both SSA and DMS ($AOD_{SSA+DMS}$) and satellite-based MODIS AOD (τ_{550}) during 2003–2015, as MODIS AOD data were not available for 2000–2002 (Fig. 3 and Supplementary Table 2). In general, the geographical (spatial) distributions of the downward or upward trends in $AOD_{SSA+DMS}$, which were governed mainly by AOD_{DMS}, were found to differ from those of MODIS AOD. In general, MODIS AOD showed upward trends (with a mean of +0.0007 or +0.74% yr^{-1}) across the whole SH, whereas there were downward trends over most areas of the NH, except for near the Arabian Sea and the Bay of Bengal (10°N–20°N, 60°E–90°E), where a maximum of +0.0194 or 3.51% yr^{-1} was observed. Similar upward trends over the Bay of Bengal (0.07 per decade)

and the Arabian Sea were observed by Terra MODIS and the Multi-angle Imaging Spectroradiometer (MISR) during 2000–2009 (Zhang and Reid, 2010). The significant upward trend over the Indian Ocean is likely related to increases in anthropogenic emissions from India (e.g., the 0.7% yr^{-1} increase in PM_1 during 2005–2010, Klimont et al., 2017). When compared to $AOD_{SSA+DMS}$, MODIS AOD trends in the northern tropical Pacific Ocean were generally reversed (i.e., downward), especially near the western Pacific Ocean, mainly due to recent decreases in anthropogenic emissions of PM_{10} from China because of strict emissions regulation policies during 2000–2010 (−0.11% yr^{-1} decrease from 11.73 to 11.61 Tg yr^{-1}, Klimont et al., 2017).

In contrast to $AOD_{SSA+DMS}$, the weak upward trend in MODIS AOD over the SH suggests that anthropogenic effects were also non-negligible in the less polluted remote marine atmosphere of the SH (Fig. 3). In the SH, the transport of biomass burning (forest and savannah fires) aerosols may have affected aerosol loading over the oceans, as biomass burning accounted for 44% of total global PM emissions in 2010 (Klimont et al., 2017). Emissions from fires in South America, southern Africa, and Australia accounted for 52% of global biomass burning emissions during 2003–2008 (Kaiser et al., 2012) and, in addition, fire emissions from South America increased during 2000–2004 (van der Werf et al., 2006). Carbon emissions from fires in southern Africa showed upward annual trends from 2003 (500 Tg C) to 2010 (575 Tg C), suggesting a significant contribution of aerosols of continental origin to AOD over the ocean in the SH (Kaiser et al., 2012). Meanwhile, the impact of ship emissions in the SH on AOD was negligible because ship tracks (vessel densities) were concentrated over the Northern Pacific and Northern Atlantic Oceans (Schreier, et al. 2007).

Table 2 presents the yearly and seasonal trends in $AOD_{SSA+DMS}$ for each latitude band from January 2003 to December 2015. The annual $AOD_{SSA+DMS}$ over the ocean exhibited statistically significant downward trends at 0°–10°N (−0.70% yr^{-1}), 30°N–40°N (−0.56% yr^{-1}), and 40°S–50°S (−0.66% yr^{-1}), and upward trends at 10°–20° in both the NH (0.21% yr^{-1}) and the SH (0.41% yr^{-1}). The trends exhibited distinct seasonal differences. A strong upward trend (1.35% yr^{-1}) was predicted at 10°S–20°S in JJA, whereas a strong downward trend was predicted at 0°–10°N in MAM. In general, however, $AOD_{SSA+DMS}$ showed negligible seasonal trends over large areas.

Temporal variations in AOD_{SSA}, AOD_{DMS}, and $A_{ODSSA+DMS}$ during the study period (2000–2015) are given in Supplementary Fig. 2 and Supplementary Tables 3 and 4. In the NH, AOD_{SSA} was highest over the latitude band of 10°N–20°N (0.032) and lowest at 30°N–40°N (0.023) and was related to the distribution of SSA emissions in these regions. The $AOD_{SSA+DMS}$ in both the NH and SH were highest in the latitude band of 10°–20° (0.090–0.112 for the NH and 0.087–0.110 for the SH), regardless of season. The $AOD_{SSA+DMS}$ (0.10) was highest over the same area as AOD_{SSA}, while its lowest value (0.05) occurred at 50°N–60°N (Supplementary Table 4). This minimum was a result of the relatively low AOD_{DMS} (0.026) at 50°N–60°N, caused by the low sea-to-air DMS flux. Meanwhile, MODIS AOD (0.192) at 0°–10°N during DJF was significantly higher than those (0.067–0.149) at 20°N–60°N by a factor of 1.7, while that (0.164) at 0°–10°S during JJA was higher than those (0.085–0.091) at 20°S–60°S by a factor of 2.8 (Supplementary Table 5). This may be related to summer biomass burning, such as forest and savannah fires in North Africa (0°–30°N) and southern Africa (0°–35°S), respectively[42]. The highest MODIS AOD was observed at 10°N–20°N during JJA, probably due to natural marine sources as the highest $AOD_{SSA+DMS}$ was predicted for the same area. In addition, natural marine AODs (i.e., $AOD_{SSA+DMS}$) at low latitudes were generally higher than those at mid-latitudes. MODIS AOD in the latitude bands of 20°N–40°N (with a mean of 0.18) seemed to be affected by the transport of anthropogenic PM emitted from China and South Asia (which accounted for 35% of global PM emissions in 2010, Klimont et al., 2017), especially over the western Pacific Ocean.

Indirect estimation of the contribution of SSA emissions (AOD_{SSA}) to atmospheric aerosol loading (MODIS AOD) over the marine atmosphere was also carried out in this study (Fig. 4 and Supplementary Table 6). In general, the contribution of AOD_{SSA} exhibited a gradual decrease over most oceans from 2003 to 2015. The contribution of AOD_{SSA} (43%) in the SH during 2003–2015 was significantly higher than that (27%) in the NH. For example, the contributions of SSA to MODIS AOD in the SH increased from 28% at 0°–10°S to 62% at 50S°–60°S, with the largest contribution (approximately 90%) observed in the Southern Ocean, while those in the NH ranged from 23% (30°N–40°N) to 35% (50N°–60°N). The relatively high contribution of SSA emissions (AOD_{SSA}) and total natural marine sources ($AOD_{SSA+DMS}$) in the Southern Ocean was possibly due to the reduced impacts from anthropogenic

sources in continental regions. In addition, there was a significant seasonal variation in SSA contributions. The SSA contributions in SON and DJF in the NH (31–38%) were higher than those in MAM and JJA (20–23%), and vice versa for the SH (47–55% in MAM and JJA and 34–36% in SON and DJF). The mean total contributions of primary SSA and the secondary contributions from DMS oxidation ($AOD_{SSA+DMS}$) to MODIS AOD in the NH and SH were 60 and 86%, respectively, implying that the secondary marine source (DMS oxidation) was important for atmospheric aerosol loading (Supplementary Table 7). In a previous study, the contribution of biogenic sulfur (DMS) in the fine particle mode over the Atlantic Ocean was less than 35% of the excess sulfur in the NH (0°–60°N), and about 60% in the SH (0°–35°S, Patris et al., 2000). Our mean DMS-derived sulfate contributions to atmospheric aerosol loading were similar to these values, 33% in the NH and 44% in the SH (54% for 0°–30°S).

4. Summary and Conclusions

The long-term trends in the sea-to-air emissions of marine aerosols (SSAs) and their precursor (DMS) during 2000–2015 were characterized using a SSA source function and an empirical DMS algorithm, based on satellite observations and model simulations. Their annual trends were also analyzed with the MK test. In addition, the AODs derived from direct SSA production (i.e., AOD_{SSA}), and secondary aerosol production by DMS oxidation (e.g., AOD_{DMS}), were evaluated using the OPAC model. These AODs were then compared to satellite-derived MODIS AOD to quantify the contributions of marine-based aerosols to atmospheric aerosol loading. Yearly global mean anomalies in DMS fluxes and AOD derived from SSA showed statistically significant downward trends during the recent global warming hiatus, whereas SSA emissions and AOD derived from DMS oxidation did not. In terms of regional trends, strong increases in SSA emissions occurred over the tropical southeastern Pacific, the northeastern Pacific, the North Atlantic, the Arabian Sea, and the Bay of Bengal, whereas strong downward trends occurred over the central Pacific, the Indian Ocean, and near the Caribbean Sea. On the other hand, DMS fluxes exhibited a clear decreasing trend over most oceans from 2000 to 2015. The

trends in SSA emissions and DMS fluxes were likely caused primarily by SSW changes, suggesting reduced impacts of SST during the recent global warming hiatus period.

The yearly trends in AOD_{SSA}, AOD_{DMS}, and $AOD_{SSA+DMS}$ were different than those of SSA emissions and DMS fluxes, due to the different physical properties of AOD. In general, the geographical (spatial) distributions of the downward or upward trends in $AOD_{SSA+DMS}$ were governed mainly by AOD_{DMS}. In terms of the contributions of natural primary marine aerosols to MODIS AOD, AOD_{SSA} over oceans during 2003–2015 accounted for approximately 28–62% (SH) and 23–35% (NH) of MODIS AOD, with the largest contribution (~90%) observed in the Southern Ocean, as this region is less impacted by anthropogenic sources in continental regions. The significant upward (in the Indian Ocean) and downward trends (near the western Pacific Ocean) in MODIS AOD are likely related to increasing and decreasing anthropogenic PM emissions from India and China, respectively. In addition, the long-range transport of biomass burning aerosols from forest and savannah fires, which are concentrated in North Africa and southern Africa during summer, can significantly reduce the relative contributions of marine aerosols, even in the SH. The mean contributions of total marine aerosols, including secondary production, were 60% in the NH and 87% in the SH.

Acknowledgments

This work was supported by the National Research Foundation of Korea (NRF) grant funded by the Korea government (MSIP) (2017R1A2B2003616). This research was also supported by Basic Science Research Program through the National Research Foundation of Korea (NRF) funded by the Ministry of Science, ICT and future Planning (2015R1A2A1A10053971).

The English in this document has been checked by at least two professional editors, both native speakers of English. For a certificate, please see:

http://www.textcheck.com/certificate/k4sRXr

412 **References**

413

414 Anttila, P. and Tuovinen, J.-P.: Trends of primary and secondary pollutant concentrations in Finland in
415 1994-2007, Atmos. Environ., 44, 30-41, 2010.
416 Archer, S.D., Ragni, M., Webster, R., Airs, R.L., and Geider, R.J.: Dimethyl sulfoniopropionate and
417 dimethyl sulfide production in response to photoinhibition in Emiliania huxleyi, Limnol.
418 Oceanogr. 55, 1579-1589, 2010.
419 Blanchard, D.C.: The electrification of the atmosphere by particles from bubbles in the sea, Prog.
420 Oceanogr., 1, 73–202, doi:10.1016/0079-6611(63)90004-1, 1963.
421 Carslaw, D.C.: Evidence of an increasing NO_2/NO_x emissions ratio from road traffic emissions, Atmos.
422 Environ., 39, 4793-4802, 2005.
423 Choi, Y.-N., Song, S.-K., Han, S.-B., Son, Y.-B., and Park, Y.-H.: Estimations and long-term trend of
424 sea-to-air dimethyl sulphide (DMS) flux using satellite observation data, Ocean Polar Res., 39,
425 181-194, 2017.
426 Clarke, A.D., Owens, S.R., and Zhou, J.: An ultrafine sea-salt flux from breaking waves: Implications
427 for cloud condensation nuclei in the remote marine atmosphere, J. Geophys. Res., 111, D06202,
428 doi:10.1029/2005JD006565, 2006.
429 Cropp, R.A., Norbury, J., Gabric, A.J., and Braddock, R.D.: Modeling dimethylsulphide production in
430 the upper ocean,. Global Biogeochem. Cy., 18, GB3005. doi:10.1029/2003GB002126, 2004.
431 de Leeuw, G., Andreas, E. L., Anguelova, M. D., Fairall, C. W., Lewis, E. R., O'Dowd, C., Schulz, M.,
432 and Schwartz, S. E.: Production flux of sea spray aerosol, Review, J. Geophys. Res., 49, RG2001,
433 doi:10.1029/2010RG000349, 2011.
434 England, M., McGregor, S., Spence, P., Meehl, G., Timmermann, A., Cai, W., Gupta, A., McPhaden,
435 M., Purich, A., and Santoso, A.: Recent intensification of wind-driven circulation in the Pacific
436 and the ongoing warming hiatus, Nat. Clim. Change, 4, 222-227, 2014.
437 Folland, C.K., Renwick, J.A., Salinger, M.J., and Mullan, A.B.: Relative influences of the Interdecadal
438 Pacific Oscillation and ENSO on the South Pacific Convergence Zone, Geophys. Res. Lett., 29,
439 211-214, 2002.

440 Gabric, A.J., Cropp, R.A., McTainsh, G., and Braddock. R.: Coupling between cycles of phytoplankton
441 biomass and aerosol optical depth as derived from SeaWiFS time series in the subantarctic
442 Southern Ocean, Geophys. Res. Lett., 29, 1112, doi:10.1029/2001GL013545, 2002.
443 Gabric, A.J., Simó, R., Cropp, R.A., Hirst, A.C., and Dachs, J.: Modeling estimates of the global
444 emission of dimethylsulfide under enhanced greenhouse conditions, Global Biogeochem. Cy.,
445 18:GB2014. doi:10.1029/2003GB002183, 2004.
446 Gong, S. L.: A parameterization of sea-salt aerosol source function for sub- and super-micron particles,
447 Global Biogeochem. Cy., 17, 1097, doi:10.1029/2003GB002079, 2003.
448 Grythe, H., Ström, J., Krejci, R., Quinn, P., and Stohl, A.: A review of sea-spray aerosol source functions
449 using a large global set of sea salt aerosol concentration measurements, Atmos. Chem. Phys.,
450 14, 1277. 2014.
451 Hammond, M.L., Beaulieu, C., Sahu, S.K., and Henson, S.A.: Assessing trends and uncertainties in
452 satellite-era ocean chlorophyll using space-time modeling, Global Biogeochem. Cy., 31, 1103–
453 1117, doi:10.1002/2016GB005600, 2017.
454 Hess, M., Koepke, P., and Schult, I.: Optical properties of aerosols and clouds: the software package
455 OPAC, B. Am. Meteorol. Soc., 79, 831-844, 1998.
456 IPCC: Climate Change 2013: The Physical Science Basis. Contribution of Working Group I to the Fifth
457 Assessment Report of the Intergovernmental Panel on Climate Change [Stocker, T.F., D. Qin,
458 G.-K. Plattner, M. Tignor, S.K. Allen, J. Boschung, A. Nauels, Y. Xia, V. Bex and P.M. Midgley
459 (eds.)], Cambridge University Press, Cambridge, United Kingdom and New York, NY, USA,
460 1535 pp., 2013.
461 Jaeglé, L., Quinn, P. K., Bates, T. S., Alexander, B., and Lin, J.-T.: Global distribution of sea salt
462 aerosols: new constraints from in situ and remote sensing observations, Atmos. Chem. Phys.,
463 11, 3137, 2011.
464 Kaiser, J.W., A. Heil, A., Andreae, M.O., A. Benedetti, A., Chubarova, N., Jones, L., Morcrette, J.-J.,
465 Razinger, M., Schultz, M.G., Suttie, M., and van der Werf, G.R.: Biomass burning emissions
466 estimated with a global fire assimilation system based on observed fire radiative power,
467 Biogeosciences, 9, 527–554. doi:10.5194/bg-9-527-2012, 2012.

468 Kettle, A.J., Andreae, M.O., Amouroux, D., Andreae, T.W., Bates, T.S., Berresheim, H., Bingemer, H.,
469 Boniforti, R., Curran, M.A.J., DiTullio, G.R., Helas, G., Jones, G.B., Keller, M.D., Kiene, R.P.,
470 Leck, C., Levasseur, M., Malin, G., Maspero, M., Matrai, P., McTaggart, A.R., Mihalopoulos,
471 N., Nguyen, B.C., Novo, A., Putaud, J.P., Rapsomanikis, S., Roberts, G., Schebeske, G., Sharma,
472 S., Simó, R., Staubes, R., Turner, and S., Uher, G.: A global database of sea surface
473 dimethylsulfide (DMS) measurements and a procedure to predict sea surface DMS as a function
474 of latitude, longitude, and month, Global Biogeochem. Cy., 13, 399-444. 1999.
475 Kettle, A.J. and Andreae, M.O.: Flux of dimethylsulfide from the oceans: A comparison of updated data
476 sets and flux models, J. Geophys. Res., 105, 26793-26808, 2000.
477 Kettle, H. and Merchant, C.J.: Systematic errors in global air-sea CO_2 flux caused by temporal averaging
478 of sea-level pressure, Atmos. Chem. Phys., 5, 1459-1466, 2005.
479 Klimont, Z., Kupiainen, K., Heyes, C., Purohit, P., Cofala, J., Rafaj, P., Borken-Kleefeld, J., and Schöpp,
480 W.: Global anthropogenic emissions of particulate matter including black carbon, Atmos. Chem.
481 Phys., 17, 8681-8723, 2017.
482 Korhonen, H., Carslaw, K., Spracklen, D., Mann, G., and Woodhouse, M.: Influence of oceanic dimethyl
483 sulfide emissions on cloud condensation nuclei concentrations and seasonality over the remote
484 Southern Hemisphere oceans: A global model study, J. Geophys. Res., 113, D15204,
485 doi:10.1029/2007JD009718, 2008.
486 Lana, A., Bell, T.G., Simó, R., Vallina, S.M., Ballabrera-Poy, J., Kettle, A.J., Dachs, J., Bopp, L.,
487 Saltzman, E.S., Stefels, J., Johnson, J.E., and Liss, P.S.: An updated climatology of surface
488 dimethlysulfide concentrations and emission fluxes in the global ocean, Global Biogeochem.
489 Cy., 25, GB1004, doi:10.1029/2010GB003850, 2011.
490 Lewis, E.R., and Schwartz, S.E.: Sea Salt Aerosol Production: Mechanisms, Methods, Measurements
491 and Models—A Critical Review. Geophysical Monograph 152, AGU, Washington, D. C., 2004.
492 Liss, P.S. and Merlivat, L.: Air-sea Exchange Rates: Introduction and Synthesis. In: Buat-Menard, P.
493 (Ed.), The Role of Air-Sea Exchange in Geochemical Cycling. D. Reidel, Dordrecht, Holland,
494 pp. 113-127. 1986.

Mårtensson, E. M., Nilsson, E.D., de Leeuw, G., Cohen, L.H., and Hansson., H.C.: Laboratory simulations of the primary marine aerosol production, J. Geophys. Res., 108, 4297, doi:10.1029/2002JD002263, 2003.

Monahan, E. C., Spiel, D. E., and Davidson, K. L.: A model of marine aerosol generation via whitecaps and wave disruption, Oceanic Whitecaps and Their Role in Air-Sea Exchange Processes, edited by: Monahan, E. C., G. MacNiocaill, Reidel, Dordrecht, the Netherlands, 167–174, 1986.

NOAA (National Oceanic and Atmospheric Administration): Extended reconstructed sea surface temperature (ERSST.v3b). National Climatic Data Center. Accessed March 2014. www.ncdc.noaa.gov/ersst. 2014.

Ovadnevaite, J., Manders, A., de Leeuw, G., Ceburnis, D., Monahan, C., Partanen, A.-I., Korhonen, H., and O'Dowd, C. D.: A sea spray aerosol flux parameterization encapsulating wave state. Atmos. Chem. Phys., 14, 1837–1852, doi:10.5194/acp-14-1837-2014, 2014.

Patris, N., Mihalopoulos, N., Baboukas, E.D., and Jouzel, J.: Isotopic composition of sulphur in size-resolved marine aerosols above the Atlantic Ocean, J. Geophys. Res., 105, 14449-14457. 2000.

Quenzel, H. and Müller, H.: Optical Properties of Single Mie Particles: Diagrams of Intensity-, Extinction-, Scattering-, and Absorption Efficiencies. vol. 34. Universität München, Meteorologisches Institut, Wiss. Mit. Nr. (Available from Meteorologisches Institut, Theresienstraße 37, D-80333 München, Germany, 59 pp.), 1978.

Salter, M. E., Nilsson, E. D., Butcher, A., and Bilde, M.: On the seawater temperature dependence of the sea spray aerosol generated by a continuous plunging jet, J. Geophys. Res., 119, 9052-9072 doi:10.1002/2013JD021376, 2014.

Saltzman, E., Savoie, D., Prospero, J., and Zika, R.: Methanesulfonic acid and non-sea-salt sulfate Pacific air: regional and seasonal variations, J. Atmos. Chem., 4. 227-240, 1986.

Saltzman, E.S., King, D.B., Holmen, K., and Leck, C.: Experimental determination of the diffusion coefficient of dimethylsulfide in water, J. Geophys. Res., 98, 16481-16486, 1993.

Schreier, M., Mannstein, H., Eyring, V., and Bovensmann, H.: Global ship track distribution and radiative forcing from 1 year of AATSR data, Geophys. Res. Lett., 34. L17814, doi:10.1029/2007GL030664, 2007.

523 Simmonds, P.G., Derwent, R.G., Manning, A.L., and Spain, G.: Significant growth in surface ozone at
524 Mace Head, Ireland, 1987-2003, Atmos. Environ., 38, 4769-4778, 2004.
525 Simó, R. and Dachs, J.: Global ocean emission of dimethylsulfide predicted from biogeophysical data,
526 Global Biogeochem. Cy., 16, 1078. doi:10.1029/2001GB001829, 2002.
527 Smith, M. H. and Harrison, N. M.: The sea spray generation function, J. Aerosol Sci., 29, suppl. 1, S189–
528 S190, doi:10.1016/S0021-8502(98)00280-8, 1998.
529 Van der Werf, G.R., Randerson, J.T., Giglio, L., Collatz, G.J., Kasibhatla, P.S., and Arellano, Jr., A.F.:
530 Interannual variability in global biomass burning emissions from 1997 to 2004, Atmos. Chem.
531 Phys., 6, 3423–3441, 2006.
532 Verma, S., Boucher, O., Reddy, M., Upadhyaya, H., Van, P., Binkowski, F., and Sharma, O.:
533 Tropospheric distribution of sulphate aerosols mass and number concentration during INDOEX-
534 IFP and its transport over the Indian Ocean: a GCM study, Atmos. Chem. Phys., 12, 6185–6196.
535 doi:10.5194/acp-12-6185-2012, 2012.
536 Wanninkhof, R.: Relationship between wind speed and gas exchange over the ocean, J. Geophys. Res.
537 97, 7373-7382, 1992.
538 Yang, Y., Russell, L., Lou, S., Lamjiri, M., Liu, Y., Singh, B., and Ghan, S.: Changes in sea salt
539 emissions enhance ENSO variability, J. Climate, 29, 8575-8588, 2016.
540 Zhang, J. and Reid, J.S.: A decadal regional and global trend analysis of the aerosol optical depth using
541 a data-assimilation grade over-water MODIS and Level 2 MISR aerosol products, Atmos. Chem.
542 Phys., 10, 10949–10963. doi:10.5194/acp-10-10949-2010, 2010.

Atmos. Chem. Phys. Discuss., https://doi.org/10.5194/acp-2018-322
Manuscript under review for journal Atmos. Chem. Phys.
Discussion started: 2 May 2018

Atmospheric Chemistry and Physics Discussions

543

Table 1. Summary of Mann–Kendall (MK) statistics of annual trends in sea spray aerosol (SSA) emissions (μg m^{-2} yr^{-1}) for each latitude band (10° interval) over the global ocean during the study period (2000–2015).

Latitude	All				MAM			JJA			SON			DJF		
	Q[a]	p[b]	Avg[c]	Std[d]	Q	p	Avg	Q	p	Avg	Q	p	Avg	Q	p	Avg
Northern Hemisphere																
50°-60°	**74.4**[*]	2.19	2671	688	**64**	5.53	1546	11.6	1.51	718	**-58.6**	-1.18	3245	**465.9**	17.43	5811
40°-50°	-4.5	-0.1	3180	885	1.3	0.05	1957	-7.7	-0.63	1221	-111.1	-2.05	3109	112.8	1.33	6387
30°-40°	**-69.5**	-1.7	3391	818	-35	-1.43	2002	-39.1	-1.06	3198	**-99.5**	-3.34	2127	-188.8	-2.96	6172
20°-30°	-29.3	-0.28	9664	694	47.1	0.68	7226	**-165.2**	-1.22	12182	-194.9	-1.49	10909	**269.4**	3.54	8331
10°-20°	**-161**	-0.59	25103	1584	-100.9	-0.39	23331	-217.6	-0.77	26461	**-330.5**	-1.5	18241	-67	-0.2	31998
0°-10°	**-232.7**	-1.35	15549	1462	**-358.5**	-1.79	15873	**-194.2**	-1.11	16091	**-174**	-1.55	10371	-132.3	-0.65	19571
Southern Hemisphere																
0°-10°	-17.3	-0.1	16720	1313	**-82.7**	-0.58	12757	19.2	0.08	24169	-18.7	-0.11	17237	**-94.1**	-0.74	12597
10°-20°	53.7	0.25	22253	1564	**-177.3**	-0.78	20129	**324.9**	1.1	30813	87.5	0.41	23755	-25.6	-0.19	14241
20°-30°	-30.8	-0.3	8828	1014	-44.3	-0.3	10240	-3.3	-0.05	5972	-39.5	-0.57	7330	5.8	0.05	11575
30°-40°	-42.4	-1.33	2748	448	-24.8	-1.35	1973	**-107.7**	-2.23	3847	-14	-0.42	2533	-32.5	-1.13	2637
40°-50°	13.6	0.14	9431	946	-22.4	-0.22	8897	-15.2	-0.14	9922	112.5	1.18	9885	-82.2	-0.81	8992
50°-60°	**154.1**	1.61	9600	1653	123.9	0.79	11487	152.6	2.23	8142	**318.6**	4.94	10187	137.8	2.1	9249

[a] Q is a slope of long-term trend calculated using the non-parametric Sen's method.

[b] %/yr.

[c] Average.

[d] Standard deviation.

[*] Values in bold are statistically significant with 90% confidence level.

Atmos. Chem. Phys. Discuss., https://doi.org/10.5194/acp-2018-322
Manuscript under review for journal Atmos. Chem. Phys.
Discussion started: 2 May 2018

Atmospheric Chemistry and Physics Discussions

Table 2. Summary of MK statistics of annual trends in aerosol optical depths (AODs) derived from SSA and dimethyl sulfide (DMS) ($AOD_{SSA+DMS}$) for each latitude band (10° interval) over the ocean during 2003–2015.

Latitude	All				MAM			JJA			SON			DJF		
	Q[a]	p[b]	Avg[c]	Std[d]	Q	p	Avg	Q	p	Avg	Q	p	Avg	Q	p	Avg
Northern Hemisphere																
50°-60°	-4.10E-05	-0.09	0.0497	0.003	1.40E-04	0.31	0.0449	-6.20E-05	-0.14	0.0456	-4.20E-04	-0.84	0.0572	7.70E-04	1.56	0.0562
40°-50°	-2.30E-04	-0.45	0.051	0.0023	1.90E-05	0.04	0.0459	**-2.20E-04**	-0.45	0.0471	-3.10E-04	-0.6	0.0526	-9.50E-05	-0.16	0.0569
30°-40°	**-3.0E-04***	-0.56	0.0519	0.0024	-1.10E-04	-0.24	0.0458	-2.50E-04	-0.43	0.0553	**-5.00E-04**	-0.98	0.0482	-1.50E-04	-0.24	0.0569
20°-30°	-3.80E-05	-0.05	0.0737	0.0029	2.40E-04	0.36	0.0679	-4.80E-04	-0.53	0.0843	-2.00E-04	-0.27	0.0758	5.60E-04	0.99	0.066
10°-20°	**2.10E-04**	0.21	0.1008	0.0021	4.10E-04	0.4	0.1023	-2.30E-04	-0.21	0.1035	-9.30E-05	-0.1	0.0902	3.40E-04	0.32	0.1123
0°-10°	**-6.00E-04**	-0.7	0.0854	0.004	**-9.00E-04**	-1.09	0.0821	**-7.10E-04**	-0.83	0.0873	-4.80E-04	-0.64	0.076	-2.20E-04	-0.23	0.0953
Southern Hemisphere																
0°-10°	2.30E-04	0.27	0.0895	0.0024	3.00E-04	0.39	0.0791	**4.90E-04**	0.48	0.1063	3.10E-04	0.35	0.0893	**4.10E-04**	0.52	0.0795
10°-20°	**3.90E-04**	0.41	0.0987	0.0023	**5.70E-04**	0.62	0.0953	**1.40E-03**	1.35	0.1102	3.70E-04	0.38	0.1015	-6.30E-04	-0.7	0.0872
20°-30°	1.00E-05	0.01	0.0695	0.0032	-1.50E-04	-0.21	0.0731	3.80E-04	0.68	0.0569	-4.80E-06	-0.01	0.0654	4.50E-04	0.52	0.0837
30°-40°	-1.80E-04	-0.37	0.048	0.0014	-1.40E-04	-0.3	0.0465	-3.40E-04	-0.71	0.0476	**-1.70E-04**	-0.37	0.0455	-2.10E-04	-0.4	0.0525
40°-50°	**-4.40E-04**	-0.66	0.064	0.0024	**-5.10E-04**	-0.8	0.0662	-2.70E-04	-0.45	0.0567	-2.50E-04	-0.43	0.0591	-8.90E-04	-1.17	0.0711
50°-60°	-5.90E-05	-0.08	0.0683	0.0046	-2.70E-04	-0.33	0.0771	-4.00E-04	-0.76	0.0569	-9.70E-05	-0.15	0.0631	-5.30E-04	-0.72	0.0714

[a] Q is a slope of long-term trend calculated using the non-parametric Sen's method.

[b] %/yr.

[c] Average.

[d] Standard deviation.

* Values in bold are statistically significant with 90% confidence level.

Atmos. Chem. Phys. Discuss., https://doi.org/10.5194/acp-2018-322
Manuscript under review for journal Atmos. Chem. Phys.
Discussion started: 2 May 2018

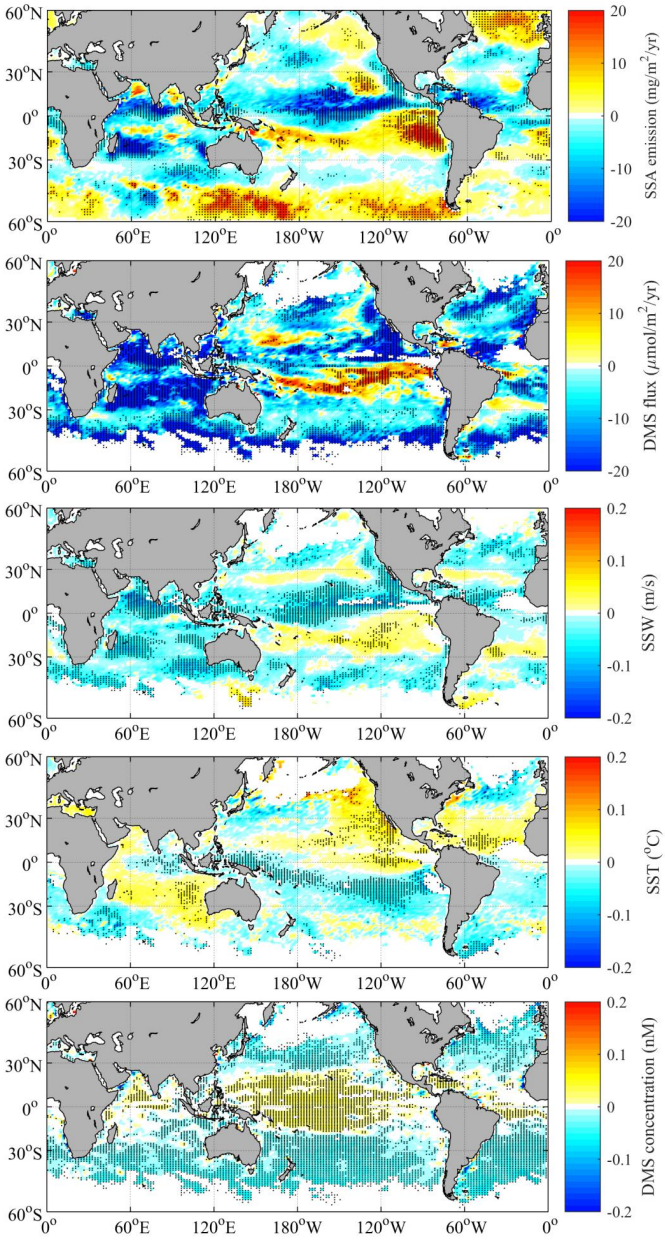

Fig. 1. Annual trends in sea spray aerosol (SSA) emissions (mg m^{-2} yr^{-1}), dimethyl sulfide (DMS) fluxes (μmol m^{-2} yr^{-1}), sea surface wind (SSW, m s^{-1}), sea surface temperature (SST, °C), and seawater DMS concentrations (nM) in the global ocean over the entire study period (2000–2015). The dots indicate significant values at the 90% confidence level.

Atmos. Chem. Phys. Discuss., https://doi.org/10.5194/acp-2018-322
Manuscript under review for journal Atmos. Chem. Phys.
Discussion started: 2 May 2018

Atmospheric Chemistry and Physics Discussions

551

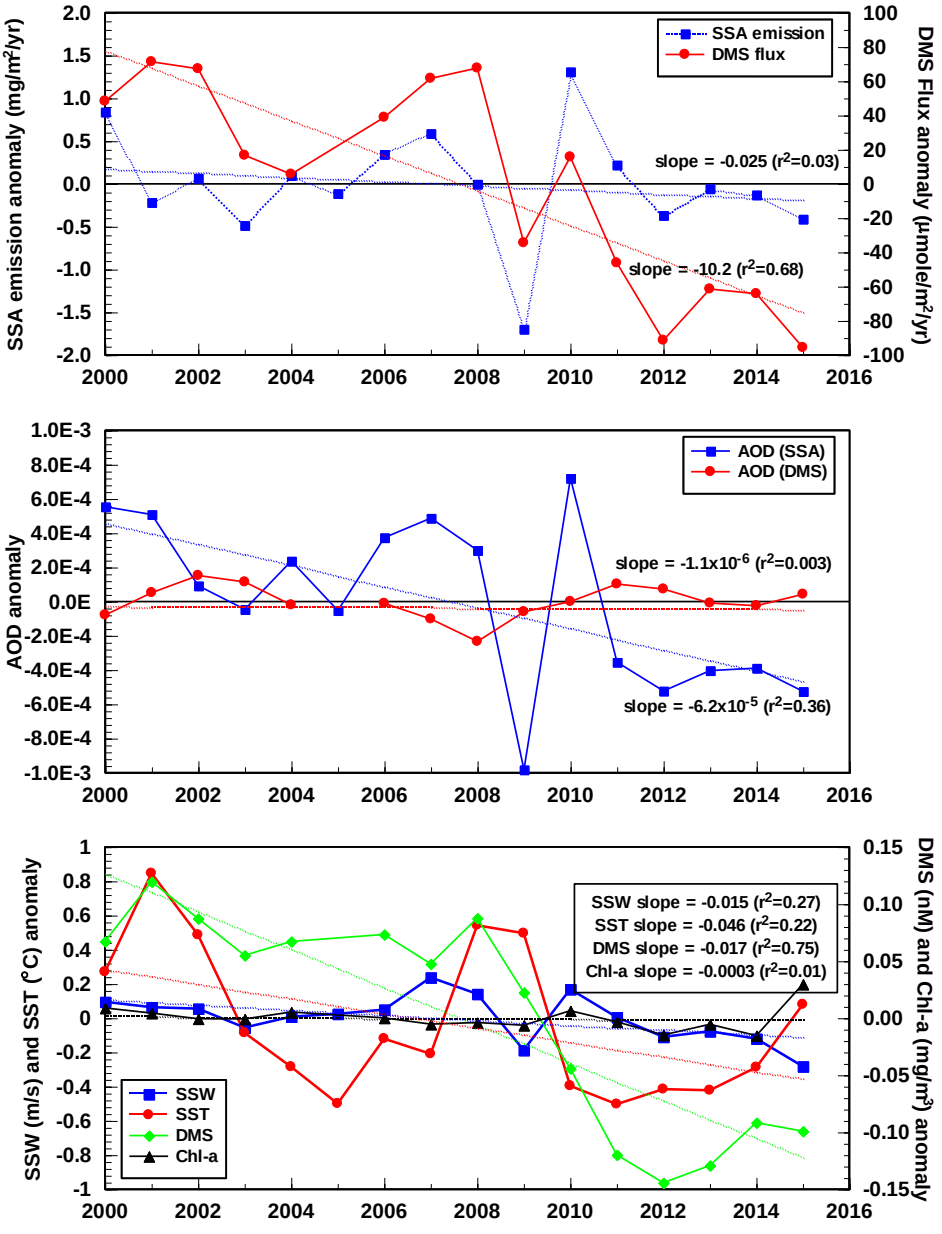

552

553 Fig. 2. Anomalies in global mean SSA emissions, DMS fluxes, aerosol optical depth derived from

554 SSA (AOD_{SSA}), AOD_{DMS}, SSW, SST, DMS concentrations, and chlorophyll-a during 2000–2015.

555

Atmos. Chem. Phys. Discuss., https://doi.org/10.5194/acp-2018-322
Manuscript under review for journal Atmos. Chem. Phys.
Discussion started: 2 May 2018

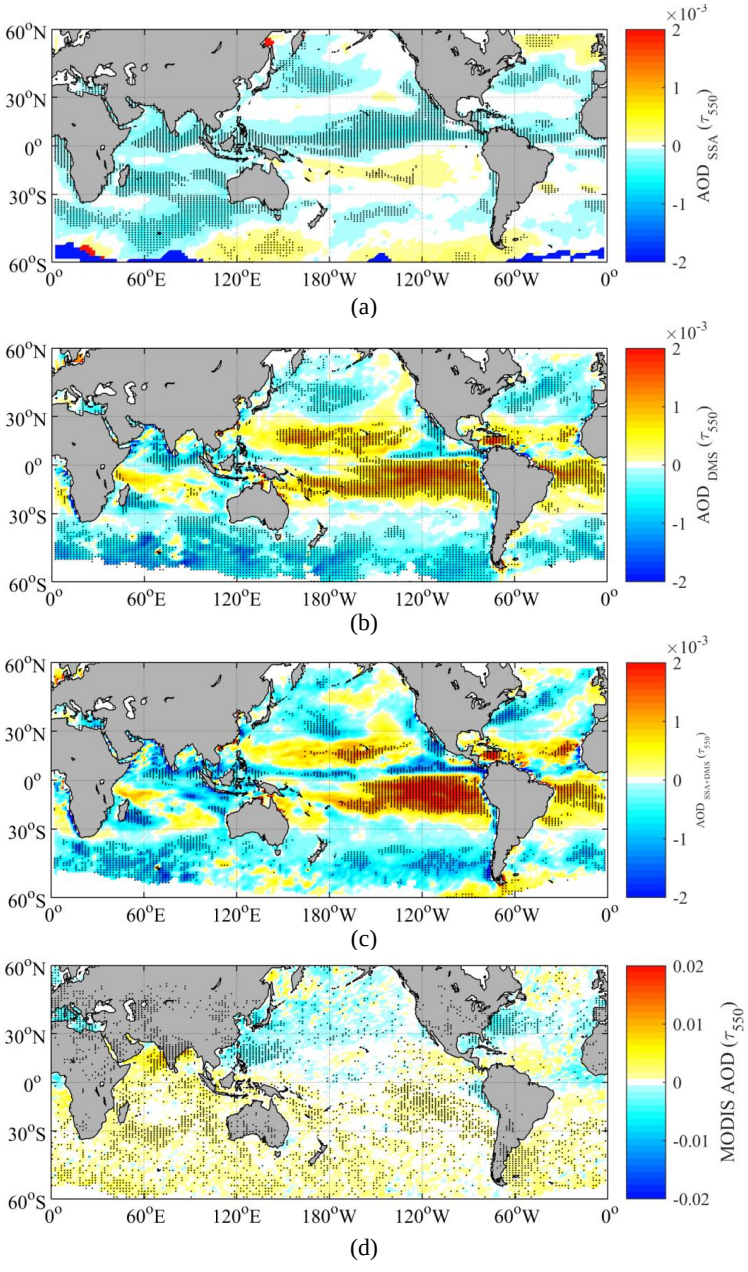

Fig. 3. Annual trends in (a) AODs (τ_{550}) derived from SSA emissions (AOD_{SSA}), (b) DMS fluxes (AOD_{DMS}) during 2000–2015, (c) AODs (τ_{550}) derived from SSA and DMS fluxes ($AOD_{SSA+DMS}$), and (d) MODIS AOD (τ_{550}) during 2003–2015. The dots indicate significant values at the 90% confidence level.

Atmos. Chem. Phys. Discuss., https://doi.org/10.5194/acp-2018-322
Manuscript under review for journal Atmos. Chem. Phys.
Discussion started: 2 May 2018

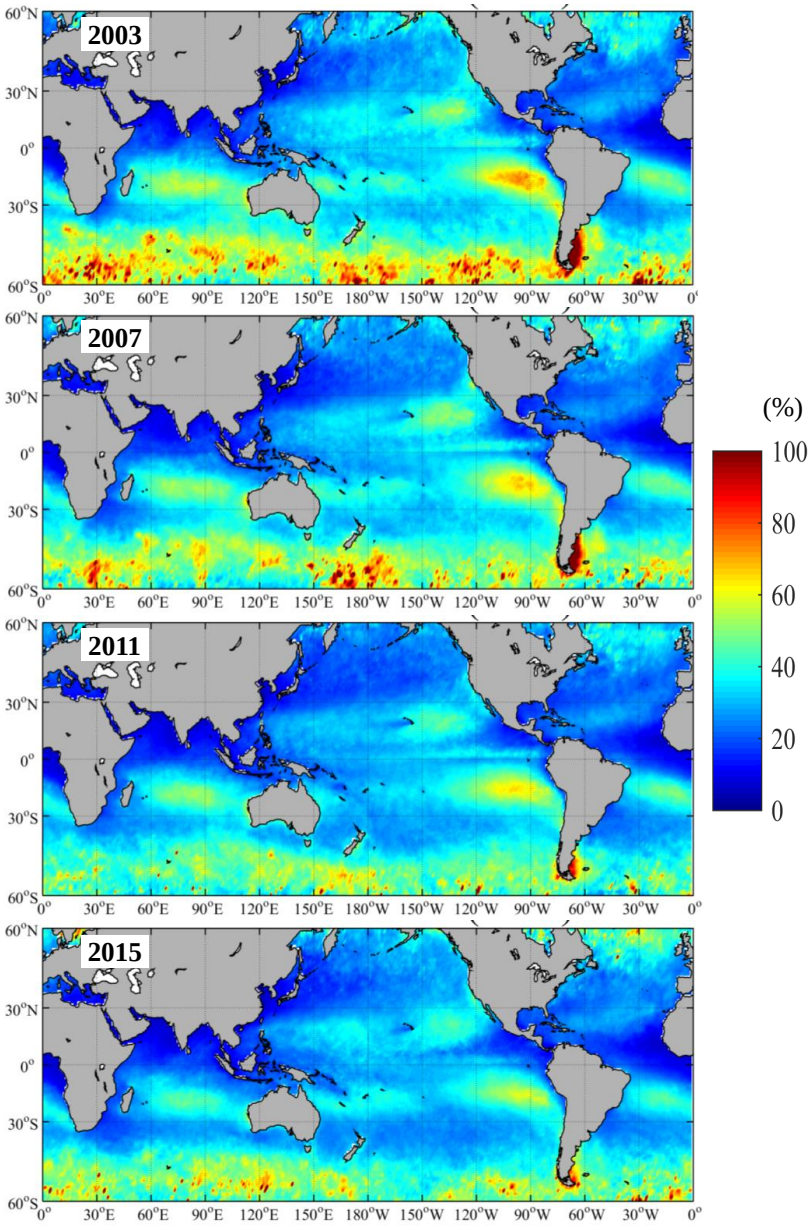

Fig. 4. Contributions (%) of AOD_{SSA} to MODIS AOD over the global ocean averaged over four years (2003, 2007, 2011, and 2015).